

## TRANSITION METAL OXIDES AS MATERIALS FOR ADDITIVE LASER MARKING ON STAINLESS STEEL

MIHAIL STOYANOV MIHALEV<sup>a,\*</sup>, CHAVDAR MOMCHILOV HARDALOV<sup>b</sup>,  
CHRISTO GEORGIEV CHRISTOV<sup>b</sup>, MONIKA RINKE<sup>c</sup>, HARALD LEISTE<sup>c</sup>

<sup>a</sup> *Technical University of Sofia, Faculty of Mechanical Engineering, Department of Precision Engineering and Measurement Instruments, 8 Kl. Ohridski blvd, 1000 Sofia, Bulgaria*

<sup>b</sup> *Technical University of Sofia, Department of Applied Physics, 8 Kl. Ohridski blvd, 1000 Sofia, Bulgaria*

<sup>c</sup> *Karlsruhe Institute of Technology, Institute of Applied Materials – Applied Materials Physics, Hermann-von-Helmholtz-Platz 1, 76344 Eggenstein-Leopoldshafen, Germany*

\* corresponding author: [mmihalev@tu-sofia.bg](mailto:mmihalev@tu-sofia.bg)

**ABSTRACT.** The product information plays an important role in the improvement of the manufacturing, allowing the tracking of the part through the full life cycle. Laser marking is one of the most versatile techniques for this purpose. In this paper, a modification of the powder bed selective laser melting for additive laser marking of stainless steel parts is presented. This modification is based on the use of only one transition metal oxide chemically bonded to the stainless steel substrate, without using any additional materials and cleaning substances. The resulting additive coatings, produced from initial MoO<sub>3</sub> and WO<sub>3</sub> powders, show strong adhesion, high hardness, long durability and a high optical contrast. For estimation of the chemical and structural properties, the Raman and X-Ray Diffraction (XRD) spectroscopy have been implemented. A computer model of the process of the laser melting and re-solidification has been developed as well. A comparative analysis of the properties of both (MoO<sub>3</sub> and WO<sub>3</sub>) additive coatings has been performed. An attempt for a qualitative explanation of the thermo-chemical phenomena during the marking process has been undertaken.

**KEYWORDS:** additive laser marking; transition metal oxides; X-Ray diffraction; Raman scattering; finite element modeling.

### 1. INTRODUCTION

Nowadays, the product information becomes more and more important due to the globalization of the world industry. A device can be designed in one country, produced in second one and assembled in a third one. This kind of production requires a consistent system for identification and classification of the products.

The correct marking plays a key role for identification of details. The requirements for marked details have been standardized [1, 2] and accepted by a number of industries. According to the standard [1], the inscription must not change its mechanical and optical properties during the whole product lifecycle. From technological point of view, the marking coating is expected to have a high optical contrast in a broad spectral range as well as a good adhesion to the substrate and a high durability.

One of the most versatile techniques is the laser marking. However, an inscription of metal parts, especially of stainless steel, with standard material subtractive methods like laser ablation is a challenge for the laser marking due to the low contrast, change of the substrate properties during the laser treatment and emerging of habitats of micro-flora and fauna, which makes it unacceptable for marking of medical instruments. The overcoming of most of the mentioned disadvantages can be achieved by an additive

marking process. TherMark, Irvine, CA, USA invented and patented method, named by the authors “laser bonding” [3].

In this work, a modification of the laser bonding (in terms of TherMark), which needs solely one transition metal oxide for preparation of an additive dark colored coating, well chemically bonded to the stainless steel substrate, without any additional materials and cleaning substances, is suggested. This modification can be considered as an additive manufacturing process similar to the “Powder Bed Selective Laser Melting” in terms of ISO/ASTM 52900 [4]. Hereinafter it will be named “Additive Laser Marking”, abbreviated as ALM.

### 2. MATERIALS AND METHODS

#### 2.1. MATERIALS

A plate of the grade 304 stainless steel has been chosen as a substrate. Two transition metal oxides have been implemented as chemical substances for the laser marking: 99.9% MoO<sub>3</sub> and WO<sub>3</sub> powders. The oxides have been diluted in alcohol for pre-coating by using a spray gun.

#### 2.2. EXPERIMENTAL EQUIPMENT

The equipment for the production of a marking coating is based on an industrial laser engraver

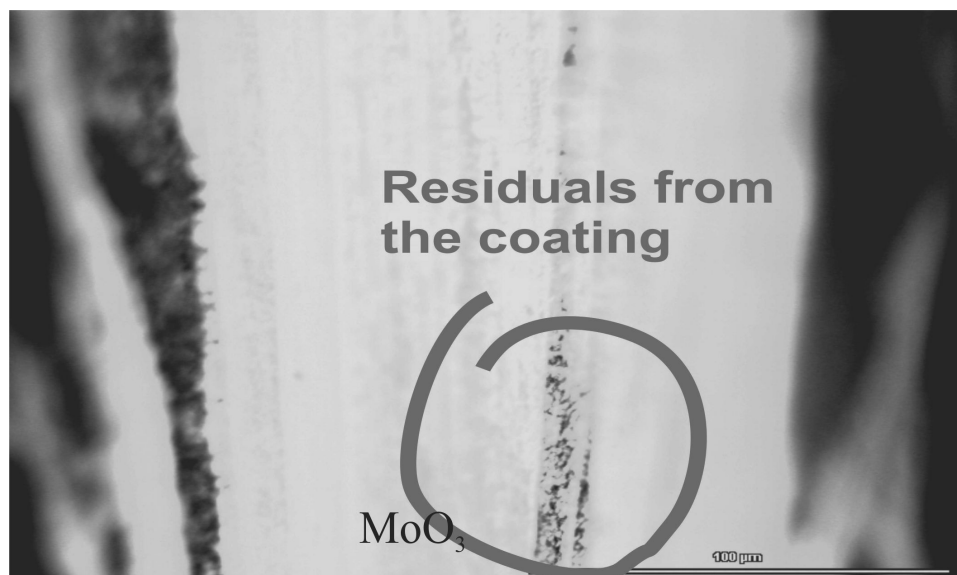


FIGURE 1. Microphotograph of scratch trace at final stage of 100 N.

Coating material	Critical load	Hardness
WO <sub>3</sub>	15 N	550 NV
MoO <sub>3</sub>	> 100 N	251 NV

TABLE 1. Critical load and hardness of the coatings.

JQ6090 with a sealed CO<sub>2</sub> laser tube with a maximal output power of 80 W. The power used during the experiments has been chosen to typically be 50 W. The laser beam has been directed by the build-in XY fly optics moving system (with a high scanning velocity of up to 30 m/min, typically 10–15 m/min) to the 50 mm focusing ZnSe lens. The lens forms a focal spot of approximately 200 μm on the sample [5–7].

### 2.3. PROPERTIES MEASUREMENT AND MICROSTRUCTURE CHARACTERIZATION

Two types of samples have been prepared — a “dot” sample with a fixed laser beam and a “scanned-laser-beam” sample, where the laser beam scans line-by-line a rectangular area of 10 × 10 mm. The hatching spacing was chosen to be 0.05 mm. Raman spectroscopy (IAM-AWP, KIT, Karlsruhe, Germany, excitation by an Ar<sup>+</sup> laser  $\lambda = 514.5$  nm) has been applied for the chemical characterization of the obtained coating for both types of samples. An X-ray diffractometer Seifert 3050 (located in IAM-AWP, KIT, Germany) has been used for analyzing of ALM MoO<sub>3</sub> and WO<sub>3</sub> “scanned-laser-beam” coating samples. The adhesion and hardness of the coatings have been characterized through the scratch tester CSEM Revetest (IAM-AWP, KIT, Karlsruhe, Germany).

The optical measurements have been performed at Bulgarian Academy of Sciences — Institute of Solid State Physics using a Perkin-Elmer Lambda 1050 UV/VIS/IR spectrophotometer.

## 3. RESULTS

All measurements have been performed “ex-situ”, i.e. after deposition or after the additive coating. The identification of the chemical compounds from the Raman and XRD spectra has been achieved by a comparison with spectra data bases and cited references.

### 3.1. MECHANICAL AND OPTICAL PROPERTIES OF THE CO<sub>2</sub> SCANNED-BEAM-LASER SAMPLE

#### 3.1.1. ADHESION AND HARDNESS

##### OF CO<sub>2</sub> SCANNED-BEAM-LASER SAMPLE

Samples of ALM MoO<sub>3</sub> and WO<sub>3</sub> on stainless steel, prepared under different technological conditions, have been examined. The scratch test has been performed with a linear increasing load (load rate 100 N/min, feed rate 5.7 mm/min, total experiment time 1 min). The averaged results for hardness are presented in Table 1. Both types of scanned-beam-laser samples show very high hardness against penetration. The scratch test of MoO<sub>3</sub> reveals a larger critical load than the WO<sub>3</sub> one. Even at a load of 100 N, no failure of the MoO<sub>3</sub> scanned-beam-laser sample has been observed, while WO<sub>3</sub> fails at 15 N only. Figure 1 represents the scratch test results for the MoO<sub>3</sub> coating in the load range around 100 N. From the photograph, it can be seen that a residue of the MoO<sub>3</sub> coating is still visible in the substrate at the final stage of the scratch test.

#### 3.1.2. OPTICAL CONTRAST

##### OF MOO<sub>3</sub> AND WO<sub>3</sub> COATINGS

Figure 2 presents the optical contrast between the coating and substrate, which is an important characteristic for the barcode and 2D code reading as required by the standard [8]. Accordingly, the contrast has been calculated as the ratio of the difference between the reflection coefficients of the coating and substrate to the reflection coefficient of the substrate.

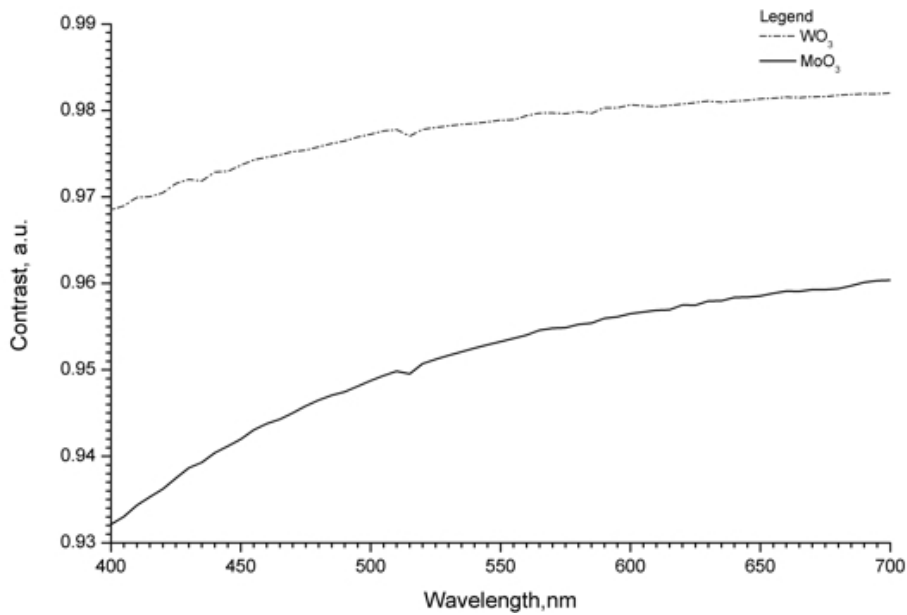


FIGURE 2. Spectral contrast distribution.

As it can be seen, both coatings have a high and relatively constant contrast in the whole visible region, where the most of the barcode readers operate. The  $\text{WO}_3$  coating shows a higher contrast (between 0.97 and 0.98) and a more uniform spectral distribution in comparison with the  $\text{MoO}_3$  coating (with a larger contrast dispersion between 0.93 and 0.96).

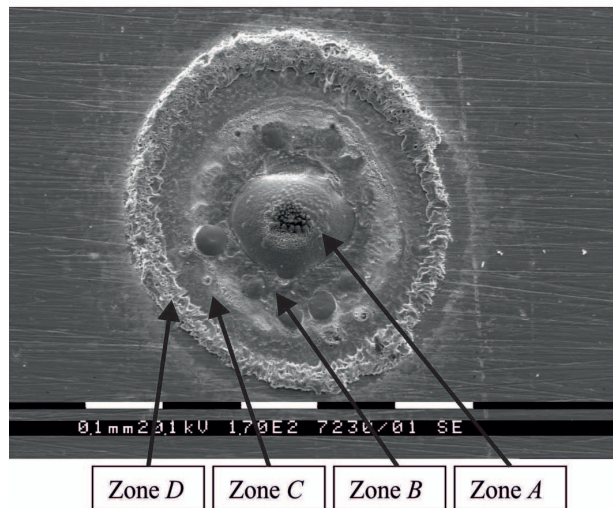
### 3.2. "DOT" SAMPLES

#### 3.2.1. MORPHOLOGY OF A "DOT" SAMPLE — MOLYBDENUM TRIOXIDE

The most typical pattern is presented in Figure 3, it was obtained at  $\text{CO}_2$  laser irradiation times between 10 and 100 ms, being relevant to the technology processes of laser marking. Under the laser radiation, the  $\text{MoO}_3$  powder undergoes melting and subsequent re-solidification processes. Fringe-like zones can be observed in the SEM image, denoted as *A*, *B*, *C* and *D*. The dimensions of "dots" depend strongly on the  $\text{CO}_2$  laser irradiation time. In our experiments, the "dots" diameters vary from 200 to 400  $\mu\text{m}$ , according to laser pulses between 1 and 1000 ms.

#### 3.2.2. MICRO-RAMAN SPECTROSCOPY OF MOLYBDENUM TRIOXIDE

Figure 4 presents a qualitative presentation of the chemical change in the coating in two experiments with long irradiation times of 100 and 1000 ms, correspondingly. In the spectra in both figures, Raman peaks of different molybdenum oxides ( $\text{MoO}_3$  at 995, 819, 665, 283, 158  $\text{cm}^{-1}$  and  $\text{Mo}_4\text{O}_{11}$  at 380, 337 and 229  $\text{cm}^{-1}$ ) [9, 10] can be observed in zone *D*. Besides molybdenum oxides in higher intermediate stoichiometric phases, additional peaks have been observed, which were assigned to a new chemical compound —  $\text{Fe}_2(\text{MoO}_4)_3$  (peaks at 969, 930, 787, 693  $\text{cm}^{-1}$ ) — in

FIGURE 3. SEM image of a  $\text{MoO}_3$  "dot".

zones *C* and *D* at both irradiation times [11]. Typically, the full width at a half maximum (FWHM) of all peaks decreases from the zone *A* to zone *D*. In the center (zone *A*), no noticeable Raman peaks can be observed. The increase of the irradiation time leads to a broadening of all peaks in all zones (Figure 4, 1000 ms).

#### 3.2.3. MORPHOLOGY OF A TUNGSTEN TRIOXIDE "DOT" SAMPLE

Figure 5 presents a typical image of a  $\text{WO}_3$  "dot" sample acquired by the microscope of the micro-Raman spectrometer. The irradiation times of the  $\text{CO}_2$  pulses vary between 50 and 500 ms, relevant to the additive marking technology. The morphology of a  $\text{WO}_3$  "dot" is similar to the morphology of a  $\text{MoO}_3$  "dot" and fringe-like zones can be observed, denoted in the manner of previous case with *A*, *B*, *C* and *D*.

### 3.2.4. MICRO-RAMAN SPECTROSCOPY

#### OF A TUNGSTEN TRIOXIDE “DOT” SAMPLE

In the spectra acquired under irradiation times of 100 and 500 ms, peaks of the following substances have been identified (Figure 6):  $\text{WO}_3$  (238, 270, 326, 638, 672, 807, 955  $\text{cm}^{-1}$ , [12], iron oxides  $\text{FeO}$  (303  $\text{cm}^{-1}$ ),  $\text{Fe}_2\text{O}_3$  (535, 635  $\text{cm}^{-1}$ ) [13],  $\text{Fe}_3\text{O}_4$  (713  $\text{cm}^{-1}$ ) [14, 15] and  $\text{FeWO}_4$  (680, 876, 881  $\text{cm}^{-1}$ ) [15]. A broadening of the peaks with an increase of the irradiation time has been also noted. In the center of all “dots”, no remarkable Raman peaks can be detected. With the distance from the center to the periphery, the FWHM decreases so that in the remote zone  $D$ , the peaks are the narrowest.

### 3.3. “SCANNED-LASER-BEAM” SAMPLES

#### 3.3.1. XRD SPECTROSCOPY

**Molybdenum trioxide.** Figure 7 shows a typical XRD spectrum of a coating obtained by scanned  $\text{CO}_2$  laser beam. The following peaks have been identified: (i) molybdenum oxides —  $\text{MoO}_3$  and  $\text{MoO}_2$  [16]; (ii) stable stoichiometric phases of higher intermediate molybdenum oxides —  $\text{Mo}_4\text{O}_{11}$ ,  $\text{Mo}_8\text{O}_{23}$  [16]; (iii) a new iron containing chemical compound —  $\text{Fe}_2(\text{MoO}_4)_3$  [16]. Characteristic peaks of stainless steel substrate (iv) have also been observed.

**Tungsten trioxide.** The typical XRD pattern of a scanned-beam  $\text{CO}_2$  laser sample, obtained from initial  $\text{WO}_3$ , shown in Figure 8, reveals similar behavior to this of  $\text{MoO}_3$ . Peaks of  $\text{WO}_3$ , iron oxides ( $\text{FeO}$ ,  $\text{Fe}_2\text{O}_3$ ,  $\text{Fe}_3\text{O}_4$ ) [16], higher intermediate tungsten oxides ( $\text{W}_4\text{O}_{11}$ ,  $\text{W}_{18}\text{O}_{49}$ ) [16] and stainless steel have been identified.

#### 3.3.2. MICRO-RAMAN SPECTROSCOPY

Additionally to the XRD, a Micro-Raman spectroscopy of the scanned-beam  $\text{CO}_2$  laser sample has been performed.

**Molybdenum trioxide.** Results of the Micro-Raman spectroscopy of molybdenum samples are presented in Figure 9. In the spectra, nearly all typical peaks, identified in the case of “dot” samples, have also been observed, they were assigned to  $\text{MoO}_3$  and  $\text{Mo}_4\text{O}_{11}$ . Unlike to the “dot” sample, a peak at 354  $\text{cm}^{-1}$ , assigned to  $\text{MoO}_2$ , has been identified. Weak peaks from iron containing compounds have been also identified: (i)  $\text{Fe}_2\text{O}_3$  (120, 235  $\text{cm}^{-1}$ ), (ii)  $\text{Fe}_3\text{O}_4$  (315  $\text{cm}^{-1}$ ) and (iii)  $\text{Fe}_2(\text{MoO}_4)_3$  (430, 942  $\text{cm}^{-1}$ ). All peaks are broadened like the peaks in the zone  $A$  and  $B$  in the case of “dot” samples.

**Tungsten trioxide.** Figure 10 presents the spectra of coatings, obtained from the initial  $\text{WO}_3$  powder with a scanned  $\text{CO}_2$  laser beam. Peaks assigned to  $\text{WO}_3$  at 330, 695 and 945  $\text{cm}^{-1}$  have been identified. Iron oxide, as in the case of the coating from  $\text{MoO}_3$  powder, has also been observed:  $\text{Fe}_2\text{O}_3$  (224, 406,

679  $\text{cm}^{-1}$ ). A peak at 878  $\text{cm}^{-1}$  has been detected and assigned to  $\text{FeWO}_4$ .

## 4. MODELING APPROACH

The following model for the explanation of the fringe-like structure of the  $\text{MoO}_3$  dots has been created. The governing equations describing the melt flow and heat transfer are as follows [17–21]:

- continuity equation

$$\frac{\partial(\rho u)}{\partial x} + \frac{\partial(\rho v)}{\partial y} = 0; \quad (1)$$

- momentum equation in  $x$  direction

$$\frac{\partial u}{\partial t} + u \nabla u = \frac{1}{\rho} \frac{\partial p}{\partial x} + \mu \delta u; \quad (2)$$

- momentum equation in  $y$  direction

$$\frac{\partial v}{\partial t} + v \nabla v = \frac{1}{\rho} \frac{\partial p}{\partial y} + \mu \delta v + g \beta (T - T_M); \quad (3)$$

- energy equation

$$\frac{\partial T}{\partial t} + u \frac{\partial T}{\partial x} + v \frac{\partial T}{\partial y} = k \Delta T; \quad (4)$$

The PDE system has been solved under the following boundary conditions at the surface:

- velocity condition

$$v = 0; \quad (5)$$

- laser power space distribution

$$q = I(t) e^{-\left(\frac{x-x_0}{f}\right)^2}. \quad (6)$$

In the equations,  $u$  and  $v$  are the  $x$  and  $y$  components of the velocity field correspondingly, and  $t, x, y$  are the time and space coordinates in the two-dimensional (2-D) model. Here,  $T$  is the temperature,  $p$  is the pressure,  $\rho$  is the density of the material,  $\mu$  is the viscosity,  $k$  is the thermal diffusion coefficient,  $g$  is the gravity acceleration, and  $T_M$  is the melting temperature. The parameter  $f$  in (6) denotes the focal spot radius ( $f = 0.1$  mm in the experimental setup) and  $I(t)$  is the power density in the center of the beam ( $\text{W}/\text{cm}^2$ ).

In order to account for the movement of the liquid-air interface, the Arbitrary Lagrangian-Eulerian (ALE) grid method [22] has been employed. The latent heats, natural convection (buoyancy force) and temperature dependence of the density in the mushy region have also been taken into account [23]. The developed model is in concordance with the convective model [24], describing the characteristic surface rippling of laser re-melted surfaces.

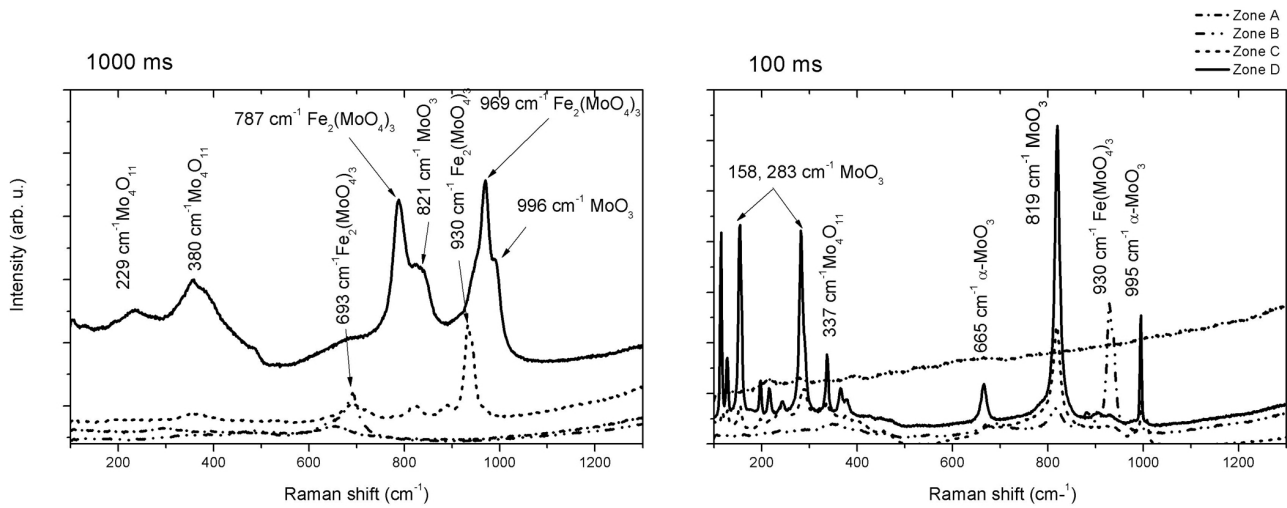


FIGURE 4. Raman spectra of two MoO<sub>3</sub> “dot” samples at different CO<sub>2</sub> irradiation times.

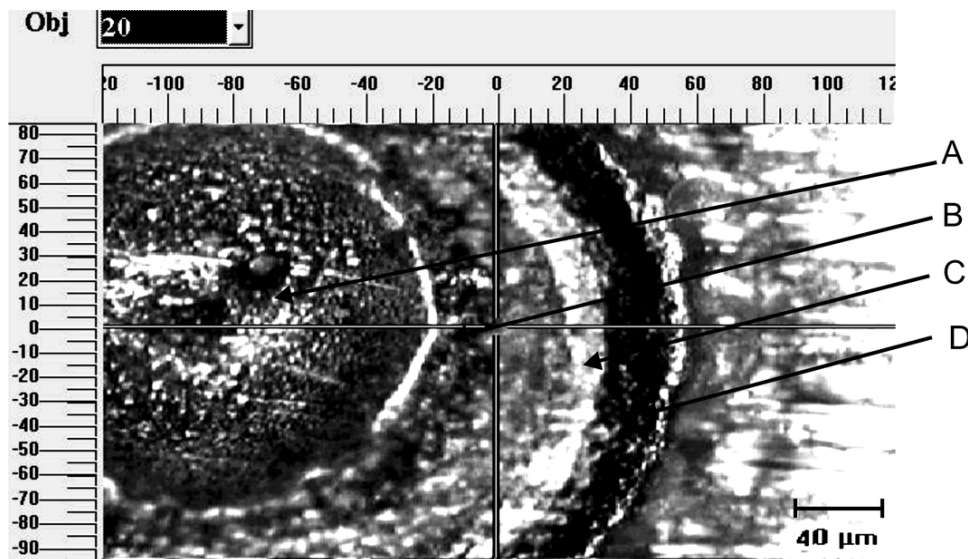


FIGURE 5. Optical image of a WO<sub>3</sub> “dot” sample.

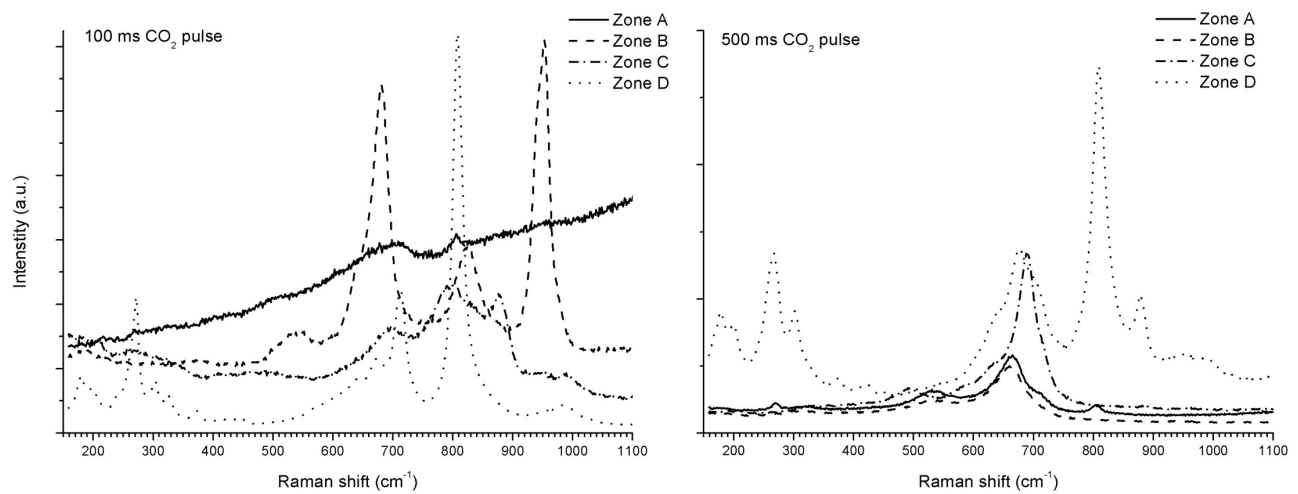


FIGURE 6. Raman spectra of two WO<sub>3</sub> “dot” samples with different CO<sub>2</sub> irradiation times.



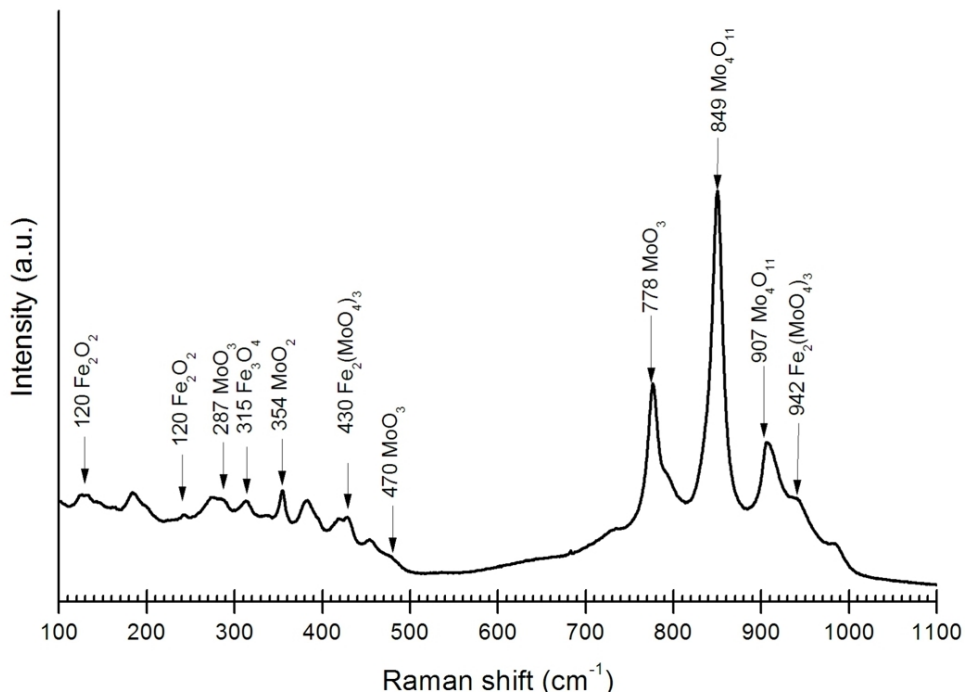


FIGURE 9. MoO<sub>3</sub>: Raman spectrum of scanned-beam cw CO<sub>2</sub> laser sample.

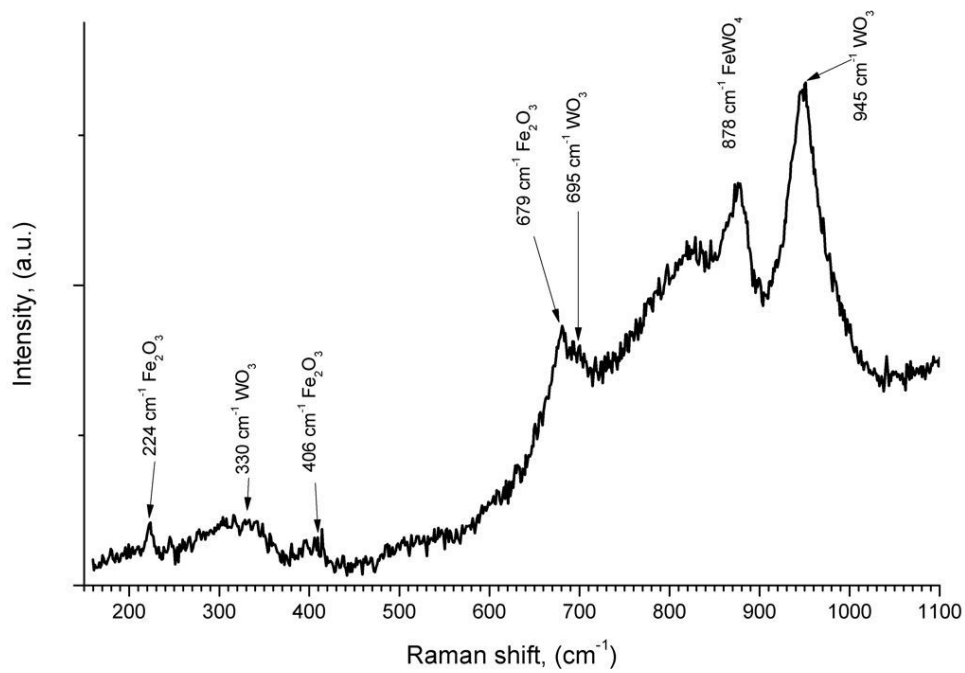


FIGURE 10. WO<sub>3</sub>: Raman spectrum of scanned-beam cw CO<sub>2</sub> laser sample.

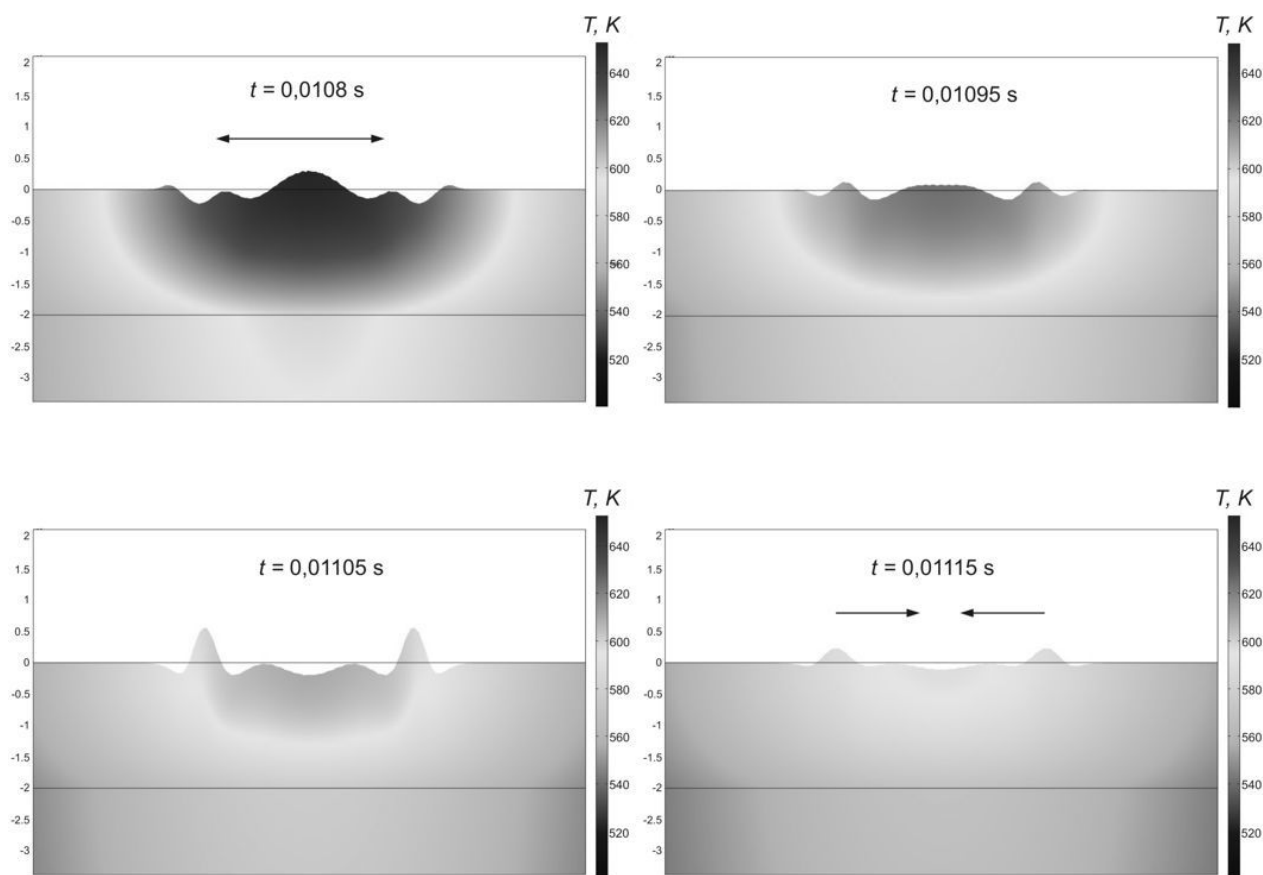
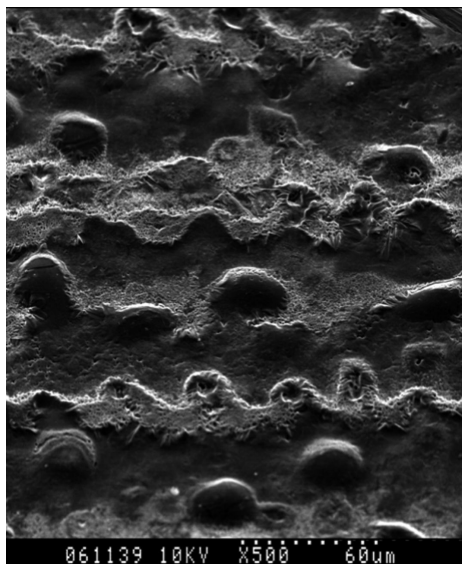


FIGURE 11. Time evolution of liquid-air surface.

FIGURE 12. SEM image of "scanned-beam" MoO<sub>3</sub> sample.

## 5. DISCUSSION

### 5.1. MORPHOLOGY

As a result of the convective flows and surface-tension gradient, the air-melt surface is rippled, building the experimentally observed characteristic fringes after the re-solidification of the melt (in Figure 3 and Figure 5

for MoO<sub>3</sub> and WO<sub>3</sub>, respectively). The computer FEM model confirms the deformation of the liquid-air surface (see Figure 11). The time evolution of this deformation reveals a behaviour of a hydro-dynamical wave, propagating from the centre to the periphery of the "dot" and back, thus modeling the solidification process, as shown in Figure 11. This surface hydro-dynamical wave could explain the experimentally observed different circular fringes on the surface of the "dot" as a result of the solidification of the melt. In the case of a scanned-beam samples, the surface is rough with bubble-like structures (Figure 12). The roughness leads to a stronger light scattering, which is a desired effect for a better optical recognition of the laser marked bar/2D code, even if the barcode reader beam is not normal to the code surface.

### 5.2. ANALYSIS OF STRUCTURAL AND CHEMICAL CHANGES

#### 5.2.1. "DOT" SAMPLES

The computational model shows a different cooling rate in different zones of the "dot" due to the Gaussian distribution of the power across the laser beam. In the center (zone A), the cooling rate was evaluated to be approx.  $10^6$  K/s with irradiation times lower than 100 ms. In the remote zone D, the cooling rate has been evaluated to be at least one order lower. In the zone A, the cooling rate is high enough (see Figure 13, calculated cooling rate  $2.58 \times 10^6$  K/s) and no

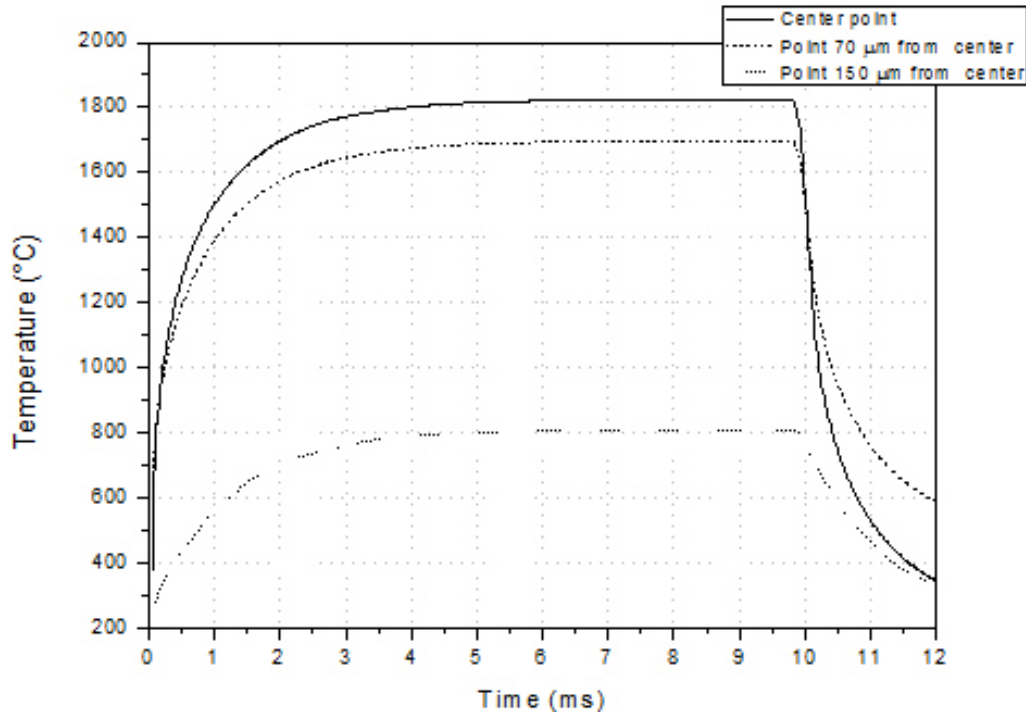


FIGURE 13. Temperature evolution in different zones of the “dot”.

nucleation of the crystalline phase occurs; accordingly, the re-solidified material is mostly amorphous [25–27]. (see the broad Raman bands without sharp peaks in this zone, Figure 4 and Figure 6). At low cooling rates (remote zones *C* and *D*, see Figure 13, calculated cooling rate  $3.7 \times 10^5$  K/s), the system mostly re-crystallizes (see narrow Raman peaks in zone *D*), thus technologically, the re-solidified material reproduces the initial powder material either  $\text{MoO}_3$  or  $\text{WO}_3$ . New chemical substances occur when laser pulse is above 100 ms. Except the initial  $\text{MoO}_3$  or  $\text{WO}_3$  materials, new stoichiometric stable intermediate oxides of transition metals have been found as well as iron containing compounds — iron (III)- and (IV)-oxides and  $\text{Fe}_2(\text{MoO}_4)_3$  or  $\text{FeWO}_4$ , all listed in Section 3. The presence of these new compounds, in our opinion, can be understood with the help of an explanation of the so called “high temperature corrosion”. The melted high oxidation grade transition metal oxides like  $\text{MoO}_3$  and  $\text{WO}_3$  act as fluxes and acids. In this way, they clean and fill-in the pores of the substrates [28–30]. According to [31], free oxygen is released, which reacts with the iron from the substrate, building iron oxides. These iron oxides interact with the melted  $\text{MoO}_3$  and as a result,  $\text{Fe}_2(\text{MoO}_4)_3$  occurs in the case of initial  $\text{MoO}_3$ . Similar mechanism also applies also  $\text{WO}_3$ , but it needs higher temperatures than the  $\text{MoO}_3$ . The new iron containing compound of Mo or W bounds chemically to the substrate and, in this way, it serves as an interface between the substrate and overlays. The presence of a chemically bounded interface as well as the amorphous character of the coating can explain the strong adhesion and the absence of a critical load in the case of initial  $\text{MoO}_3$ . The coating obtained

from initial  $\text{WO}_3$  shows a weaker adhesion to the substrate, namely due to the not fully built interface, which requires higher temperatures in comparison with  $\text{MoO}_3$ . For that reason,  $\text{WO}_3$  is considered by us as a not so perspective material for an industrial ALM, taking into account the undesired overheating and deformation of the substrates.

### 5.2.2. SCANNED-BEAM $\text{CO}_2$ LASER SAMPLE

The industrial application of the presented modification of the ALM requires scanning following an assigned topology. During the scanning, the material, in a certain point of the topology, is several times exposed to the laser radiation, because the coating area is consecutively swept by the laser beam at typical feed rates of 10–15 m/min and a hatching space of typically 0.05 mm. The laser beam spot crosses every point many times, thus manifold melting and re-solidification of the coating is observed. This way, the amorphization of the coatings, seen in the broadened Raman peaks in Figures 9 and 10, can be explained. The same chemical compounds are observed in the case of a “dot” sample with a large laser exposition time. The results from the Micro-Raman spectroscopy for both  $\text{MoO}_3$  and  $\text{WO}_3$  are confirmed by the XRD spectroscopy (see Figures 7 and 8). However, in the case of  $\text{WO}_3$  in the XRD spectrum, no iron-tungsten compounds have been identified, although  $\text{FeWO}_4$  have been found in the Micro-Raman spectra (see Figure 10). It can be reasonably assumed that the interface substrate – coating, has not been fully built, thus explaining the weaker adhesion and observed failures at relatively low loads in the scratch tests.

## 6. CONCLUSIONS

A modification of the ALM method, which needs only one transition metal oxide for a preparation of a high contrast coating over a stainless steel substrate, well chemically bonded to the metal, without any additional materials and cleaning substances, has been developed and presented. These properties of the process and the additive coatings make the method well suitable for industrial applications in the laser marking branch as well as for miscellaneous design and art purposes. The coatings show strong adhesion, high hardness, long durability and a high optical contrast. The Raman and XRD spectroscopy have been implemented for the chemical and structural analysis of samples, which was obtained under different technological conditions. A computer model of the process of the laser melting and solidification of a “dot” sample has been developed. Based on the data obtained by the Micro-Raman and XRD spectroscopy and the computer model, a heuristic attempt for an explanation of the process of the ALM has been presented.

## ACKNOWLEDGEMENTS

The support of Institute of Applied Materials/Applied Materials Physics at Karlsruhe Institute of Technology (KIT), Karlsruhe, Germany, KNMF, KIT, Karlsruhe, Germany, German Academic Exchange Service (DAAD) and of Prof. Miroslav Abrashev, Faculty of Physics, Sofia University St. Kl. Ohridski, is gratefully appreciated.

## REFERENCES

- [1] NASA standard 6002, Applying data matrix identification symbols on aerospace parts, (2002).
- [2] Military Standard MIL-STD-129, Military marking for shipment and storage, (2004).
- [3] US Patent 6075223. A high contrast surface marking.
- [4] American Society for Testing Materials. Standard Terminology for Additive Manufacturing—General Principles—Terminology; ASTM52900; ASTM International: West Conshohocken, PA, USA, 2015.
- [5] C. G. Christov, M. S. Mihalev, Ch. M. Hardalov Characterization of Thin MoO<sub>3</sub> Layers Obtained by Laser Bonding AU J.T. 14(1) (2010) 1-10.
- [6] C. Christov, M. Mihalev, Ch. Hardalov, On the dynamics of the laser bonding of MoO<sub>3</sub> on stainless steel, 27th International Congress of Turkish Physical Society, (2010) 136
- [7] C. Christov, M. Mihalev, Ch. Hardalov, Mihailov, Leiste, JPCS 514 (2014), DOI:10.1088/1742-6596/514/1/012022
- [8] ISO/IEC 17067:2013 Conformity assessment — Fundamentals of product certification and guidelines for product certification scheme.
- [9] M. Dieterle, G. Mestl, Raman spectroscopy of molybdenum oxides: Structural characterization of oxygen defects in MoO<sub>3-x</sub> by DR UV/VIS Raman spectroscopy and X-ray diffraction, PCCP 4 (2002) 812–821, DOI:10.1039/B107012F
- [10] M. Dieterle, G. Mestl, Raman spectroscopy of molybdenum oxides: Resonance Raman spectroscopic characterization of the molybdenum oxides Mo<sub>4</sub>O<sub>11</sub> and MoO<sub>2</sub>, PCCP 4 (2002) 822–826, DOI:10.1039/B107046K
- [11] Q. Xu, G. Jia, J. Zhang, Z. Feng, C. Li, Surface phase composition of iron molybdate catalysts studied by UV Raman spectroscopy, J. Phys. Chem. C 112(25) (2008) 9387–9393.
- [12] F. Zhang, H.-Q. Wang, S. Wang, J.-Y. Wang, Zh.-Ch. Zhong, Y. Jin, Structures and optical properties of tungsten oxide thin films deposited by magnetron sputtering of WO<sub>3</sub> bulk: Effects of annealing temperatures, Chin. Phys. B 23(9) (2014) 098105-098106.
- [13] S.-H. Shim, Th. S. Duffy, Raman spectroscopy of Fe<sub>2</sub>O<sub>3</sub> to 62 GPa, Am. Mineral. 87 (2001) 318–326
- [14] O.. Shebanova. P. Lazor, Raman study of magnetite (Fe<sub>3</sub>O<sub>4</sub>): laser-induced thermal effects and oxidation, J. Raman Spectrosc. 34 (2003) 845 – 852.
- [15] Online database of Raman samples of minerals. <http://www.ruff.info> [2016-07-11].
- [16] Computer program with XRD pattern database. <http://pcpdfwin.updatestar.com/de> [2016-07-11].
- [17] F. M. White, Fluid Mechanics, fourth ed., McGraw-Hill, New York, 1999, ISBN 978-0072281927.
- [18] F. Incopera, D. de Witt, Fundamentals of Heat and Mass Transfer, fourth ed., John Wiley, New York, 1996, ISBN 978-0471304609.
- [19] P. Kundu, I. Kohen, Fluid Mechanics, third ed., Elsevier Academic Press, San Diego, 2004, ISBN 9780080470238.
- [20] A. Brent, V. Voller, K. Reid, Numer. Heat Transfer 13 (1988) 297-318, DOI:10.1080/10407788808913615
- [21] U. Duitsch, S. Schreck, M. Rohde, Experimental and numerical investigations of heat and mass transport in laser-induced modification of ceramic surfaces. International Journal of Thermophysics 24(3) (2003) 731- 40.
- [22] FEMLAB, Reference manual, Version 3.1. COMSOL AB, Stockholm, Sweden, 2003.
- [23] X.-H. Ye,, X. Chen, Three-dimensional modelling of heat transfer and fluid flow in laser full- penetration welding. Journal of Physics D: Applied Physics 35(10), (2002), 1049-1056
- [24] M. Allmen, Laser-Beam Interactions with Materials, Physical Principles and Applications, Springer Series in Materials Science, Springer Verlag Berlin Heidelberg, 1987, ISBN 978-3-642-57813-7
- [25] J. Siegel, Structural transformation dynamics in Ge films upon ultrashort laser pulses irradiation, PhD thesis, 1998. [http://www.io.csic.es/Web\\_GPL/personal\\_pages/Jan/thesis/Jan\\_thesis.pdf](http://www.io.csic.es/Web_GPL/personal_pages/Jan/thesis/Jan_thesis.pdf) [2017-08-24].
- [26] S.R. Stiffler, M.O. Thompson, P.S. Peercy, Nucleation of amorphous germanium from supercooled melts, Appl. Phys. Lett. 56 (1990) 1025-1030, DOI:10.1063/1.103326
- [27] S.R. Stiffler, M.O. Thompson, P.S. Peercy, Transient nucleation following pulsed-laser melting of thin silicon films, Phys. Rev. B 43 (1991) 9851-9855, DOI:10.1103/PhysRevB.43.9851

- [28] J. H. DeVan, Catastrophic oxidation of high temperature alloys, Oak Ridge National Laboratory – US Atomic Energy Commission, Central research library collection, 1961. <http://web.ornl.gov/info/reports/1961/3445605157442.pdf>
- [29] S. S. Brenner, Catastrophic Oxidation of Some Molybdenum Containing Alloys, *J. Electrochem. Soc.* 102(1) (1955) 16-21, doi:10.1149/1.2429980
- [30] N. Birks, G. H. Meier, Fr. S. Pettit, *Introduction to the High Temperature Oxidation of Metals*, second ed, Cambridge University Press, 2006, ISBN 9780521480420.
- [31] E. Lalik, Kinetic analysis of reduction of  $\text{MoO}_3$  to  $\text{MoO}_2$ , *Catalysis Today* 169 (2011) 85–92.